European Journal of Pharmaceutics and Biopharmaceutics xxx (2009) xxx–xxx

Contents lists available at ScienceDirect

European Journal of Pharmaceutics and Biopharmaceutics

journal homepage: www.elsevier.com/locate/ejpb

Note

Histological analysis of 70-nm silica particles-induced chronic toxicity in mice

Hikaru Nishimori [a], Masuo Kondoh [a,*], Katsuhiro Isoda [a], Shin-ichi Tsunoda [b,c], Yasuo Tsutsumi [b,c,d], Kiyohito Yagi [a]

[a] Laboratory of Bio-Functional Molecular Chemistry, Graduate School of Pharmaceutical Sciences, Osaka University, Osaka, Japan
[b] Laboratory of Pharmaceutical Proteomics, National Institute of Biomedical Innovation, Osaka, Japan
[c] The Center for Advanced Medicinal Engineering and Informatics, Osaka University, Osaka, Japan
[d] Laboratory of Toxicology, Graduate School of Pharmaceutical Sciences, Osaka University, Osaka, Japan

ARTICLE INFO

Article history:
Received 10 February 2009
Accepted in revised form 24 March 2009
Available online xxxx

Keywords:
Nanotoxicology
Silica particle
Histological analysis
Liver
Spleen

ABSTRACT

Nano-sized silica is a promising material for disease diagnosis, cosmetics and drugs. For the successful application of nano-sized material in bioscience, evaluation of nano-sized material toxicity is important. We previously found that nano-sized silica particles with a diameter of 70 nm showed acute liver failure in mice. Here, we performed histological analysis of major organs such as the liver, spleen, lung, kidney, brain and heart in mice, chronically injected with 70-nm silica particles for 4 weeks. Histological analysis revealed hepatic microgranulation and splenic megakaryocyte accumulation in these 70-nm silica particles treated mice, while the kidney, lung, brain and heart remained unaffected. Thus, liver and spleen appear to be the major target organs for toxicity by the chronic administration of the 70-nm silica particles.

1. Introduction

Recent progress in nanotechnology, the act of reducing size from the microscale to the nanoscale, has provided us with dramatic changes in industrial manufacturing and medicine. It also offers many benefits to revolutionize biotechnology, such as synthesis of new drugs with targeted delivery and regenerative medicine [1]. Reducing particle size increases surface area and makes modification of unique physicochemical properties, such as high conductivity, strength, durability, and chemical reactivity possible [2]. Thus, the nanotechnology has led to novel materials and innovations in the industry, bioscience and medicine.

Nanomaterials are already being used in bioscience and medicine, such as electronics, sunscreens, cosmetics and medicine for the purposes of diagnosis, imaging and drug delivery. For example, nano-sized silica particles are intended for the systemic and local delivery of drugs [3]. However, the toxicity of the manufactured nano-sized particles has not been fully evaluated.

We previously found that nano-sized particles with a diameter of 70 nm caused acute liver failure, while micro-sized particles with a diameter of 300 or 1000 nm did not [4]. In this study, we performed histological analysis of chronic toxicity induced by intravenous administration of 70-nm silica particles (SP70) for 4 weeks into the major organs, such as liver, lung, spleen, kidney, brain and heart of mice.

2. Materials and methods

2.1. Materials

Nano-sized silica particles with a diameter of 70 nm were obtained from Micromod Partikeltechnologie GmnH (Rostock, Germany). The surface was not modified. The mean diameters of these particles analyzed by Zetasizer (Sysmex Co., Kobe, Japan) were determined to be 55.7 nm. The particles were spherical and nonporous, and were stored at 25 mg/ml in aqueous suspension. The suspensions were thoroughly dispersed with sonication before use and diluted in water. The dispersion of the particles was confirmed by electron microscopy (data not shown). Reagents used were of research grade.

2.2. Animals

The 8-week-old BLAB/c male mice were purchased from Shimizu Laboratory Supplies Co., Ltd. (Kyoto, Japan), and housed in an environmentally controlled room at 23 ± 1.5 °C with a 12-h light/dark cycle. Mice had access to water and chow (Type MF, Oriental Yeast, Tokyo, Japan) *ad libitum*. Mice were intravenously

Abbreviations: SP70, 70-nm silica particles; HE, hematoxylin–eosin; ALT, alanine aminotransferase; HYP, hydroxyproline.

* Corresponding author. Laboratory of Bio-Functional Molecular Chemistry, Graduate School of Pharmaceutical Sciences, Osaka University, Suita, Osaka 565-0871, Japan. Tel.: +81 6 6879 8196; fax: +81 6 6879 8199.
E-mail address: masuo@phs.osaka-u.ac.jp (M. Kondoh).

0939-6411/$ - see front matter © 2009 Elsevier B.V. All rights reserved.
doi:10.1016/j.ejpb.2009.03.007

injected with vehicle or the particles twice a week for 4 weeks. On day 3 after the last injection, the mice were sacrificed, and the serum and organs were recovered. The experimental protocols conformed to the ethical guidelines of the Graduate School of Pharmaceutical Sciences, Osaka University.

2.3. Histological analysis

The liver, spleen, lung, kidney, brain and heart were removed and fixed with 4% paraformaldehyde. After sectioning, thin sections of tissues were stained with hematoxylin and eosin for histological observation.

2.4. Biochemical analysis

Serum alanine aminotransferase (ALT) was measured using a commercially available kit according to the manufacturer's protocol (Wako Pure Chemical, Osaka, Japan).

2.5. Hydroxyproline (HYP) assay

Hepatic HYP content was measured by Kivirikko's method with some modification [5]. Briefly, liver tissue was hydrolyzed in 6 M HCl at 110 °C for 24 h. The resultant supernatant was neutralized with 8 N KOH, and then 2 g of KCl and 1 ml of 0.5 M borate buffer were added, followed by a 15-min incubation at room temperature and further incubation for 15 min at 0 °C. Chloramines-T solution was then prepared and added. After additional incubation for 1 h at 0 °C, 2 ml of 3.6 M sodium thiosulfate was added, followed by incubation at 120 °C for 30 min. Next, 3 ml of toluene was added with incubation for a further 20 min at room temperature. After centrifugation, 2 ml of the resultant supernatant was added to Ehrlich's reagent, followed by incubation for 30 min at room temperature. Subsequently, absorbance was measured at 560 nm.

2.6. Statistical analysis

Statistical analysis was performed by Student's *t*-test. The level of significance was set at $p < 0.05$.

3. Results and discussion

We previously found that intravenous administration of SP70 induced liver injury through a single administration [4]. To investigate the chronic toxicity of SP70, 10 or 30 mg/kg of SP70 was intravenously injected into mice twice a week for 4 weeks at which point the livers were not injured or injured by the single injection, respectively [4]. During chronic administration, no significant differences were observed in the body weight between the vehicle and the SP70-treated group (Fig. 1) and no abnormal behaviors were detected (data not shown). Therefore, SP70 treatment did not show apparent toxicity in mice at the low dose.

Next, we performed histological analysis of tissues that are enriched with reticuloendothelial system (RES) such as the liver, spleen, and lungs and non-RES organs such as the heart, kidney and brain. As shown in Fig. 2A and B, treatment with SP70 induces hepatic microgranulation and increases splenic megakaryocyte accumulation. In contrast, the remaining RES organ, the lung, and all the non-RES organs did not show tissue injury with SP70 treatment (Fig. 2B–F). Thus, we examined a serum biochemical marker of liver injury, ALT, to confirm liver injury. SP70 treatment significantly elevated serum ALT levels (Fig. 3A), but a renal injury marker, blood urea nitrogen, was not elevated by these treatments

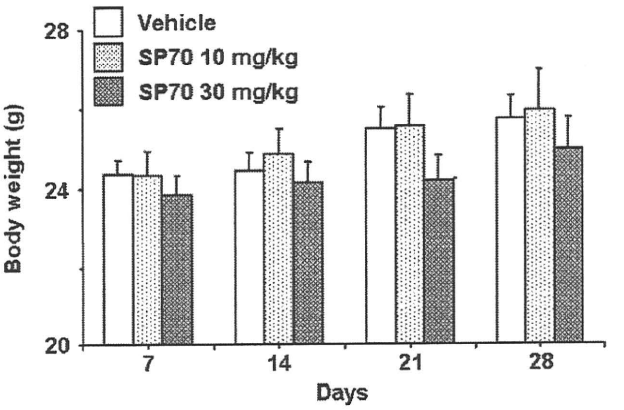

Fig. 1. Body weight changes in mice treated with SP70 for 4 weeks. Mice were intravenously administered SP70 at 0, 10 or 30 mg/kg twice a week for 4 weeks. The body weights of the treated mice were monitored on days 7, 14, 21 and 28. Each point represents mean ± SEM ($n = 5–7$).

(data not shown). Chronic hepatic injury causes liver fibrosis, finally leading to hepatic carcinoma. The chronic treatment with SP70 also elevated a marker of fibrosis, HYP, in the liver (Fig. 3B). Taken together, chronic SP70 treatment appears to injure the liver and spleen.

As innovative materials cover wide fields from industry to life science, nanomaterials have potential to improve the quality and performance of many consumer products as well as medical therapies. Thus, it is very critical in the field of nanotechnology to also assess the risk of nano-sized materials. As the use of nano-sized silica particles in cosmetics and the application in pharmaceutical research, e.g., drug delivery and molecular imaging [3,6] are increasing, we evaluated the toxicity of nano-sized silica particles. We have already found that SP70 causes acute liver injury in mice [4]. In the present study, we evaluate the influence of chronic administration of SP70 for 4 weeks on major organs by histological analysis. As the nano-sized particles are taken into RES organs such as the liver, lung and spleen, we expected that all the RES organs would be injured by chronic SP70 exposure. However, histological abnormalities in the lung were not observed. Kim et al. found that 50-nm silica particles were distributed into all the RES organs, but the amount of the distributed particles into the lung was smaller than that into the liver and spleen [7]. Therefore, the lack of histological abnormalities in the lung may be due to a lower distribution of SP70.

The underlying mechanism for histological injury in the liver and spleen remains to be elucidated. We previously found that the serum levels of inflammatory cytokines (interleukin-6 and tumor necrosis factor-α) were elevated by SP70 [4]. Uptake of SP70 by macrophages in the liver and spleen may cause the release of the cytokines from the macrophage, leading to histological abnormalities. Macrophage receptor with collagenous structure (MARCO), CD204 and CD36 are all macrophage silica particle receptors [8–10]. CD36 is expressed in macrophages of BALB/c mice [10].

In the present study, there is no observation of histological injury in lung, kidney, brain and heart. Regulation of liver and spleen injuries may be critical for the safe application of these nano-sized silica particles. Future analysis is necessary to determine tissue distribution of SP70. Extensive studies are also required to provide the basis for a new class of nanomaterials for drugs, proteins, and gene delivery applications. We are developing materials and methods to control the bio-distribution of these nano-sized silica particles.

Please cite this article in press as: H. Nishimori et al., Histological analysis of 70-nm silica particles-induced chronic toxicity in mice, Eur. J. Pharm. Biopharm. (2009), doi:10.1016/j.ejpb.2009.03.007

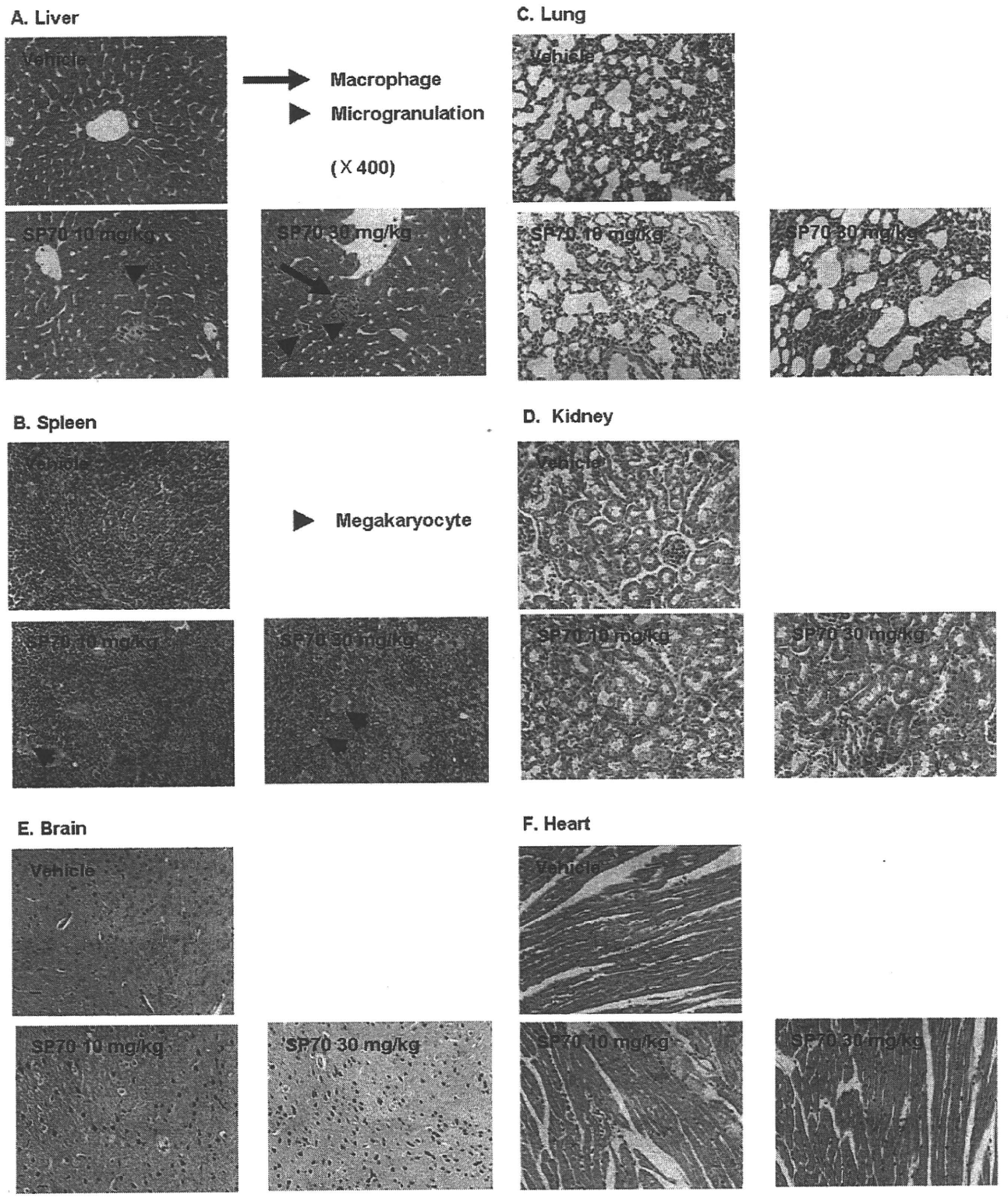

Fig. 2. Histopathological evaluation of the organs from SP70-treated mice. After chronic treatment with SP70 for 4 weeks, liver (A), spleen (B), lung (C), kidney (D), brain (E) and heart (F) were recovered and fixed with paraformaldehyde, followed by staining with hematoxylin and eosin. The arrowheads in (A) and (B) indicate microgranulation in the liver and accumulation of megakaryocyte in the spleen, respectively. The tissue sections were observed under a microscope at 400×. The pictures are representative of at least four independent sections.

Please cite this article in press as: H. Nishimori et al., Histological analysis of 70-nm silica particles-induced chronic toxicity in mice, Eur. J. Pharm. Biopharm. (2009), doi:10.1016/j.ejpb.2009.03.007

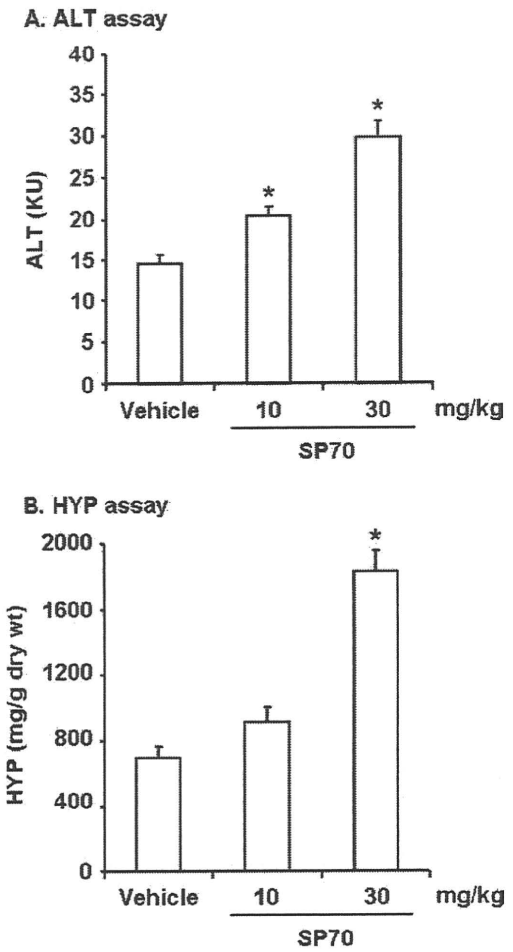

Fig. 3. Biochemical analysis of liver injury. After chronic SP70 treatment for 4 weeks, the serum and liver were collected. Then, the serum alanine aminotransferase (A) and hepatic hydroxyproline (HYP) levels (B) were measured as described in Section 2. Data are shown as mean ± SD ($n = 4$). The results are representative of at least three independent experiments. *Significant difference from the vehicle-treated group ($p < 0.05$).

Acknowledgements

We thank all members of our laboratory for their useful comments and discussion. This study is partly supported by a Grant-in-Aid from the Ministry of Health, Labor, and Welfare of Japan.

References

[1] M.C. Roco, Nanotechnology: convergence with modern biology and medicine, Curr. Opin. Biotechnol. 14 (2003) 337–346.
[2] A. Nel, T. Xia, L. Madler, N. Li, Toxic potential of materials at the nanolevel, Science 311 (2006) 622–627.
[3] M. Vallet-Regi, F. Balas, D. Arcos, Mesoporous materials for drug delivery, Angew. Chem. Int. Ed. Engl. 46 (2007) 7548–7558.
[4] H. Nishimori, M. Kondoh, K. Isoda, S. Tsunoda, Y. Tsutsumi, K. Yagi, Silica nanoparticles as hepatotoxicants, Eur. J. Pharm. Biopharm., in press, doi:10.1016/j.ejpb.2009.02.005.
[5] K.I. Kivirikko, O. Laitinen, D.J. Prockop, Modifications of a specific assay for hydroxyproline in urine, Anal. Biochem. 19 (1967) 249–255.
[6] T.J. Yoon, J.S. Kim, B.G. Kim, K.N. Yu, M.H. Cho, J.K. Lee, Multifunctional nanoparticles possessing a "magnetic motor effect" for drug or gene delivery, Angew. Chem. Int. Ed. Engl. 44 (2005) 1068–1071.
[7] J.S. Kim, T.J. Yoon, K.N. Yu, B.G. Kim, S.J. Park, H.W. Kim, K.H. Lee, S.B. Park, J.K. Lee, M.H. Cho, Toxicity and tissue distribution of magnetic nanoparticles in mice, Toxicol. Sci. 89 (2006) 338–347.
[8] L. Kobzik, Lung macrophage uptake of unopsonized environmental particulates. Role of scavenger-type receptors, J. Immunol. 155 (1995) 367–376.
[9] A. Palecanda, J. Paulauskis, E. Al-Mutairi, A. Imrich, G. Qin, H. Suzuki, T. Kodama, K. Tryggvason, H. Koziel, L. Kobzik, Role of the scavenger receptor MARCO in alveolar macrophage binding of unopsonized environmental particles, J. Exp. Med. 189 (1999) 1497–1506.
[10] R.F. Hamilton Jr., S.A. Thakur, J.K. Mayfair, A. Holian, MARCO mediates silica uptake and toxicity in alveolar macrophages from C57BL/6 mice, J. Biol. Chem. 281 (2006) 34218–34226.

Laboratory of Pharmaceutical Proteomics[1], National Institute of Biomedical Innovation (NiBio), Graduate School of Pharmaceutical Sciences[2], The Center of Advanced Medical Engineering and Informatics[3], Osaka University, Osaka, Japan

Rapid isolation of intrabody candidates by using an optimized non-immune phage antibody library

K. Nagano[1,2], S. Imai[1,2], Y. Mukai[1,2], S. Nakagawa[2,3], Y. Abe[1], H. Kamada[1,3], S. Tsunoda[1,3], Y. Tsutsumi[1,2,3]

Received November 27, 2008, accepted December 1, 2008

Shin-ichi Tsunoda, Ph.D., Laboratory of Pharmaceutical Proteomics, National Institute of Biomedical Innovation, 7-6-8 Saito-Asagi, Ibaraki, Osaka 567-0085, Japan
tsunoda@nibio.go.jp

Pharmazie 64: 238–241 (2009) *doi: 10.1691/ph.2009.8352*

Phage antibody library is a promising tool for rapidly creating *in vitro* single-chain Fv (scFv) antibodies to various antigens. The scFv can also act like a subcellularly-expressed antibody, known as intrabody, and can either be used as a novel research tool or used efficiently for targeted molecular therapy. However, there are only a few existing reports about the successful expression of scFvs as functional antibodies in the cell, mainly because poor quality scFv phage antibody libraries were used to isolate the intrabody clones. The aim of this study was to isolate intrabody-forming scFv clones from the non-immune scFv phage antibody library we have generated. Using this library, we isolated a scFv clone against the apoptosis-related intracellular protein Bid in two weeks. To evaluate the intrabody-forming quality of this anti-Bid scFv clone, we expressed it in cultured mammalian cells after fusing it with the fluorescent protein Venus. The expression of the soluble form of anti-Bid scFv-Venus fusion protein was confirmed by fluorescence microscopy analysis. These results show that our scFv phage library is not only optimized for antibody production but can also be used to efficiently generate intrabodies.

1. Introduction

Recently, it was suggested that most of the disease-related proteins or drug target proteins are located in the intracellular compartment. Therefore, it is important to elucidate the functions of these intracellular proteins to explore for novel drugs or clinical therapies and to develop ways for modulating their functions. In this respect, the intrabody technology, which is expressing an antibody in the cytoplasm, is considered to be a promising tool for analyzing the functions of subcellular proteins (Huston et al. 2001). Especially, intrabody can be useful for the analysis of post-translated modifications, because it can selectively inhibit the function of a protein. The intrabody-induced inhibition of selective protein function is different from the siRNA method, which acts by totally knocking down the protein expression. Intrabodies can also be of therapeutic use by neutralizing intracellular proteins (Miller et al. 2005; Alvarez et al. 2000). However, it has been difficult to establish the intrabody technology because the reducing cytoplasmic environment generally leads to low intrabody stability (Cattaneo et al. 1999).

Isolation of intrabodies using the phage or yeast antibody library can replace the hybridoma technique as the latter takes more time and effort (Popkov et al. 2005, 2003; Holler et al. 2000). However, only a few research groups have reported the creation of the intrabody from the non-immune phage antibody library (Rajpal et al. 2001; Colby et al. 2004), mainly because of the low quality of the antibody library.

We have already reported the construction of a high-quality non-immune phage antibody library and the optimized screening conditions to efficiently isolate a monoclonal antibody from this library (Imai et al. 2006). Thus, we believe that we can easily isolate subcellular protein-specific antibodies using this optimized non-immune phage library.

Using this phage library we first isolated a scFv clone against the apoptosis-related intracellular protein Bid, which is reported to be one of the candidate proteins relating to acute hepatitis (Yin et al. 1999). Next, we created a fusion protein between the anti-Bid scFv and the yellow fluorescence protein Venus, and then expressed this fusion protein as a soluble intrabody in cultured cells.

2. Investigations, results and discussion

We have previously reported methods to improve the quality of the non-immune murine scFv phage library and to use this phage library for the rapid isolation of monoclonal antibodies to various antigens (Imai et al. 2006). In this report, we isolated scFvs to an intracellular protein and then evaluated their intrabody formation quality. The scFv phage display library was prepared from the glycerol stock of *E. coli* TG1 containing the scFv phagemid library. The Bid-His-tag or native Bid protein was immobilized on the surface of the Biacore sensor chip and the affinity panning was performed for 3 to 5 cycles. The output/input ratio (titer of the recovered phage library after the panning/titer of phage library before the panning) was increased as the panning round was repeated (data not shown). This elevated output/input ratio indicated the en-

VL

	FR1	CDR1	FR2
scFv clone 1	DIVMTQSQKFMSTSVGDRVSVTC	KASQNVGTNVA	WYQQKPGQSPKALIY
scFv clone 2	--Q---TTSSL-A-L----TIS-	R---DISNYLN	------DGTV-L---

CDR2	FR3	CDR3	FR4
SASYRYS	GVPDRFTGSGSGTDFTLTISNVQSEDLAEYFC	QQYNSYPYT	FGGGTKLEIKR
YT-RLH-	---S--S-------YS-----LEQ--I-T---	--G-TL-L-	--A--------

VH

	FR1	CDR1	FR2
scFv clone 1	EVQLVESGGGLVKPGGSLKLSCAASGFTFS	SYAMS	WVRQTPEKRLEWVA
scFv clone 2	Q---QQ--AE-A---A-V----K---Y--T	--W-H	--K-R-GQG---IG

CDR2	FR3	CDR3	FR4
TISDGGSYTYYPDNVKG	RFTISRDNAKNNLYLQMSHLKSEDTAMYYCAR	RVGPPHYYAMDY	WGQGTSVTVSS
Y-NPSSG--K-NQKF--	KA-LTA-KSSSTA-MELRS-T---S-V---T-	WDY	-----TLQS--

Fig. 1: Amino acid sequence of the antibodies isolated from the non-immune scFv phage library by affinity panning
Amino acid sequences of the scFvs for His-Bid or native Bid, isolated from the library, were determined by DNA sequence analysis. VL; light chain variable domain of an antibody. VH; heavy chain variable domain of an antibody. FR; framework region. CDR; complementarity determining region. "–" in Fig. 1 means that the same amino acid occurs at that position in clone 2 as the clone 1

richment of the antigen-binding scFv clones. A total 96 clones were randomly picked from the post-panning output phage library and their bindings to each antigen were tested by phage ELISA. Among them, several phage clones showed higher binding to the target antigens, Bid-His or native Bid (data not shown). Analysis of the DNA sequences of these positive clones led to the identification of one Bid-His binding scFv clone and another native Bid binding scFv clone (Fig. 1). The antigenic specificity of these scFvs was investigated by phage ELISA using various proteins as antigens. The scFv clone isolated by using the Bid-His (scFv clone 1) as antigen bound not only to the Bid-His but also to the other His-tagged proteins (data not shown). Thus, scFv clone 1 may be an anti-His-tag scFv antibody. On the other hand, the scFv clone isolated by using the native Bid as antigen (scFv clone 2) bound specifically to the native Bid, but not to the His-tagged caspase-8, His-tagged importin-β, luciferase, tumor necrosis factor receptor 2 (TNFR2)-Fc-chimera, His-tagged Venus and KDR-Fc-chimera (Fig. 2). This result suggested that the scFv clone 2 was an anti-Bid specific scFv antibody.

Very often a His-tag is added to a recombinant protein for purification purposes. However, we have found that when a His-tagged protein was used as an antigen for panning, the clones of binding to the His-tag concentrated rapidly. Therefore, a modified method, which includes a step to eliminate the tag-binding clones, should be developed when having to use the His-tagged protein as antigen for panning.

In order for scFv to act as an intrabody, the most important criteria is that the scFv is expressed in the soluble form in an environment that is not suitable for antibodies (Worn and Pluckthin 2001). To evaluate the characteristics of the scFvs as intrabodies, the fluorescent protein Venus was fused to the C-terminus of the scFv and each fusion construct was subsequently analyzed for subcellular expression. The expression vector harboring the scFv clone 1 (anti-His tag scFv) or clone 2 (anti-Bid scFv) was transfected into the HEp2 cells and the expression of the fluorescent fusion protein was observed using the Olympus IX-81 fluorescence microscope. The fluorescent images 24 h after transfection revealed that both the scFv-Venus fusions were expressed in the cytoplasm (Fig. 3). Although

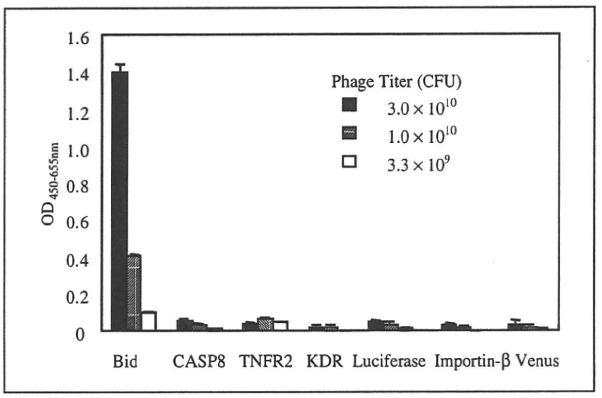

Fig. 2: Binding specificity of the isolated anti-Bid scFv antibody
Binding specificity of the anti-Bid scFv was determinded by phage ELISA. Native human Bid, His-tagged human caspase-8, human TNFR2-Fc-chimera, human KDR-Fc-chimera, luciferase, His-tagged importin-β, His-tagged Venus (50 ng each) were immobilized on the immunoassy plate and then the purified anti-Bid scFv phage (3.0×10^{10}, 1.0×10^{10} and 3.3×10^{9} CFU each) was applied to the wells. Each bar represents the mean OD450-655 nm ± SD (error bars) in three wells

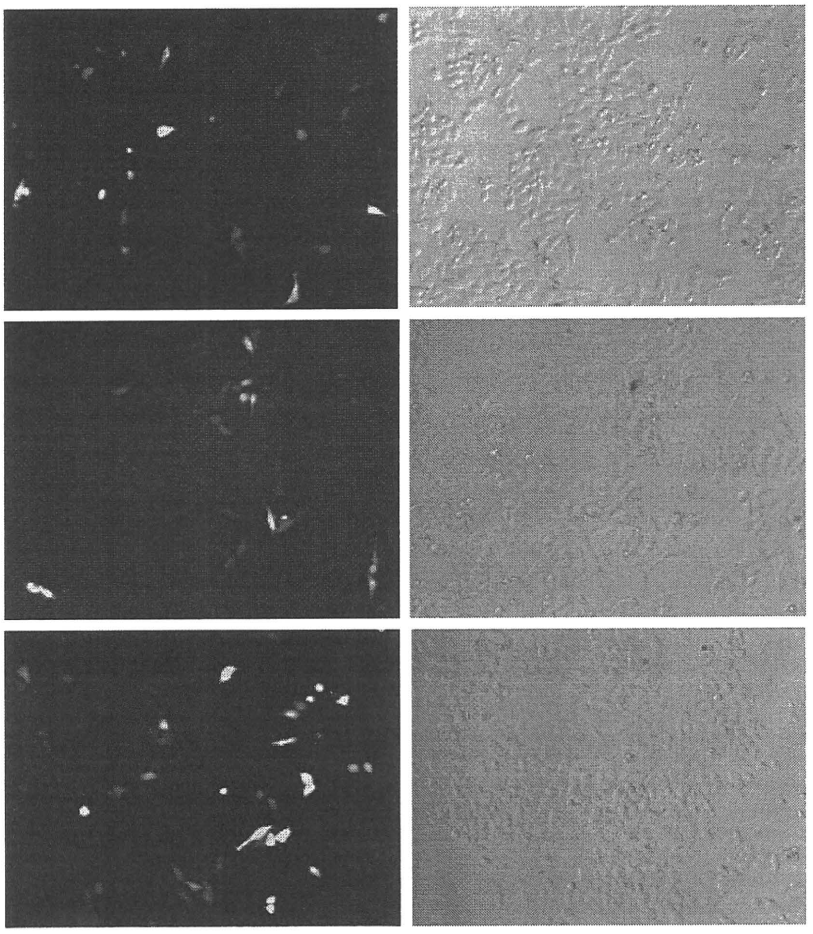

Fig. 3:
Intracellular expression of scFv-Venus fusion protein
The left panels decipt the fluorescence in the Venus (YFP) channel. The right panels show the bright-field images. The expression plasmids containing the scFv-Venus gene fusions were transiently transfected into the HEp2 cells by lipofection. A. Cells transfeted with the scFv clone1-Venus fusion construct. B. Cells transfected with the scFv clone 2-Venus fusion construct. C. Cells transfected with the pTriEx vector containing the Venus gene (control)

we will have to assess the binding of scFv to antigen in the cell and the anti-apoptotic property of the anti-Bid intrabody (clone 2) in the near future, our results suggest that we were able to isolate intrabodies from our non-immune phage antibody library.

We believe that intrabody-induced functional inhibition of Bid could be a novel therapeutic method for treating diseases, such as acute hepatitis, for which there are no treatment available (Yin et al. 1999).

It is not known which antibody can be expressed in the cytoplasm. Such fundamentally useful information can be achieved by isolating various antigen specific intrabody candidate clones using our phage library and analyzing their amino acid sequences.

3. Experimental

3.1. Cell

Human pharynx cancer cell line HEp2 cells (TKG0403, Cell Resource Center for Biomedical Research, Tohoku University) were sub-cultured in RPMI-1640 medium containing 10% fetal calf serum, 0.1% 2-mercaptoethanol and 1% sodium pyruvate. TNF-α treatment induces apoptosis in HEp2 cells (Berkova et al. 1999).

3.2. Non-immune phage scFv antibody library

Construction of the non-immune murine scFv phage library was described previously (Imai et al. 2006). The phage display library was prepared from the glycerol stock of *E. coli* TG1 containing the scFv gene library, and was immediately used for affinity panning.

3.3. Affinity panning using BIAcore

Affinity panning of antigens was performed using the microfluidic flow system based BIAcore 3000 instrument (BIAcore International AB., Uppsala, Sweden) as described previously (Imai et al. 2006). Briefly, 5 μg His-tagged Bid (Alexis Biochemicals Co., Taejon, Korea) or non-tagged Bid (Sigma-Aldrich Co., St. Louis, MO) was immobilized on the surface of the sensor chip CM3 (BIAcore). The phage library solution was injected onto the sensor chip at flow rate of 3 μL/min. After injection, the sensor chip was rinsed 10 times with the HBS-EPT (HBS-EP running buffer containing 0.05% Tween 20, Biacore). The bound phages were eluted with glycine-HCl (pH 2.0), and were treated first with glycine-NaOH (pH 11.0) and then with tris-HCl (pH 8.0) to neutralize. Recovered phages were amplified by infecting log phase TG1 cells for the next round of panning.

3.4. Phage ELISA

Single clones of affinity-panned phages were prepared from the culture supernatant of TG1 in 96 well format plate. These phages were blocked with 2% Block Ace (Dainippon Sumitomo Pharma Co., Ltd. Osaka, Japan) at 4 °C for 1 h, and then applied to the antigen-immobilized immuno-assay plate. His-tagged human caspase-8, His-tagged human-importin-β, luciferase, tumor necrosis factor receptor 2 (TNFR2)-Fc-chimera, His-tagged Venus and KDR-Fc-chimera were used as antigens. After shaking for 2~3 h at 250 rpm, the bound phage was detected using the HRP-conjugated anti-M13 monoclonal antibody (GE Healthcare Biosciences AB, Uppsala, Sweden).

3.5. Intracellular expression of scFv-Venus fusion protein

The cDNA of the fluorescent protein Venus was kindly provided by Dr. Miyawaki (Riken Brain Science Institute, Saitama, Japan). The isolated scFv genes were inserted into the NcoI and NotI digested mammalian expression vector pTriEx (Novagen), which contained the Venus gene. The resulted plasmid containing the scFv-Venus fusion protein gene was transfected into the HEp2 cells using the Lipofectamine 2000 reagent (Invitrogen, Carlsbad, CA). After 24 h incubation at 37 °C, the expression of the scFv-Venus fusion protein in the cells was observed using the Olympus IX-81 fluorescence microscope (Tokyo, Japan).

Acknowledgement: This study was supported in part by a Health and Labor Sciences Research Grant from the Ministry of Health, Labor and Welfare of Japan, and in part by a JSPS Research Fellowships for Young Scientists (No. 19–2872) from the Japan Society for the Promotion of Science.

References

Alvarez RD, Barnes MN, Gomez-Navarro J, Wang M, Strong TV, Arafat W, Arani RB, Johnson MR, Roberts BL, Siegal GP, Curiel DT (2000) A cancer gene therapy approach utilizing an anti-erbB-2 single-chain antibody-encoding adenovirus (AD21): a phase I trial. Clin Cancer Res 6: 3081–3087.

Berkova N, Lemay A, Korobko V, Shingarova L, Sagaidak L, Goupil S (1999) Tumor necrosis factor mutants with selective cytotoxic activity. Cancer Detect Prev 23: 1–7.

Cattaneo A, Biocca S (1999) The selection of intracellular antibodies. Trends Biotechnol 17: 115–121.

Colby DW, Garg P, Holden T, Chao G, Webster JM, Messer A, Ingram VM, Wittrup KD (2004) Development of a human light chain variable domain (V(L)) intracellular antibody specific for the amino terminus of huntingtin via yeast surface display. J Mol Biol 342: 901–912.

Holler PD, Holman PO, Shusta EV, O'Herrin S, Wittrup KD, Kranz DM (2000) In vitro evolution of a T cell receptor with high affinity for peptide/MHC. Proc Natl Acad Sci USA 97: 5387–5392.

Huston JS, George AJ (2001) Engineered antibodies take center stage. Hum Antibodies 10: 127–142.

Imai S, Mukai Y, Nagano K, Shibata H, Sugita T, Abe Y, Nomura T, Tsutsumi Y, Kamada H, Nakagawa S, Tsunoda S (2006) Quality enhancement of the non-immune phage scFv library to isolate effective antibodies. Biol Pharm Bull 29: 1325–1330.

Miller TW, Messer A (2005) Intrabody applications in neurological disorders: progress and future prospects. Mol Ther 12: 394–401.

Popkov M, Mage RG, Alexander C, Thundivalappil S, Barbas CF 3rd, Rader C (2003) Rabbit immune repertoires as sources for therapeutic monoclonal antibodies: the impact of kappa allotype-correlated variation in cysteine content on antibody libraries selected by phage display. J Mol Biol 325: 325–335.

Popkov M, Jendreyko N, McGavern DB, Rader C, Barbas CF 3rd (2005) Targeting tumor angiogenesis with adenovirus-delivered anti-Tie-2 intrabody. Cancer Res 6: 972–981.

Rajpal A, Turi TG (2001) Intracellular stability of anti-caspase-3 intrabodies determines efficacy in retargeting the antigen. J Biol Chem 276: 33139–33146.

Worn A, Pluckthun A (2001) Stability engineering of antibody single-chain Fv fragments. J Mol Biol 305: 989–1010.

Yin XM, Wang K, Gross A, Zhao Y, Zinkel S, Klocke B, Roth KA, Korsmeyer SJ (1999) Bid-deficient mice are resistant to Fas-induced hepatocellular apoptosis. Nature 400: 886–891.

Acta Crystallographica Section F
Structural Biology and Crystallization Communications
ISSN 1744-3091
Editors: **H. M. Einspahr and M. S. Weiss**

Crystallization and preliminary X-ray analysis of the tumour necrosis factor α–tumour necrosis factor receptor type 2 complex

Yohei Mukai, Teruya Nakamura, Yasuo Yoshioka, Shin-ichi Tsunoda, Haruhiko Kamada, Shinsaku Nakagawa, Yuriko Yamagata and Yasuo Tsutsumi

Acta Cryst. (2009). F**65**, 295–298

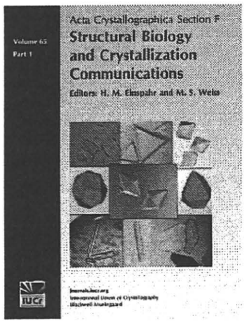

Acta Crystallographica Section F
Structural Biology and Crystallization Communications
ISSN 1744-3091

Crystallization and preliminary X-ray analysis of the tumour necrosis factor α–tumour necrosis factor receptor type 2 complex

Yohei Mukai,[a,b] Teruya Nakamura,[c] Yasuo Yoshioka,[b,d] Shin-ichi Tsunoda,[b] Haruhiko Kamada,[b] Shinsaku Nakagawa,[a] Yuriko Yamagata[c] and Yasuo Tsutsumi[a,b]*

[a]Graduate School of Pharmaceutical Sciences, Osaka University, Japan, [b]Laboratory of Pharmaceutical Proteomics, National Institute of Biomedical Innovation (NiBio), Japan, [c]Graduate School of Pharmaceutical Sciences, Kumamoto University, Japan, and [d]The Center of Advanced Medical Engineering and Informatics, Osaka University, Japan

Correspondence e-mail: ytsutsumi@phs.osaka-u.ac.jp

Received 29 September 2008
Accepted 7 February 2009

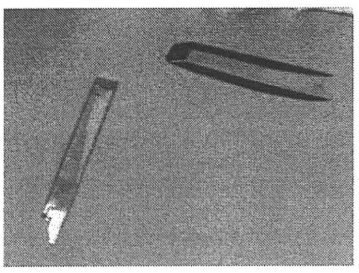

Tumour necrosis factor receptor type 2 (TNFR2, TNFRSF1B) is an essential receptor for various host-defence functions of tumour necrosis factor α (TNF). As part of studies to determine the structure of TNFR2, the formation, crystallization and preliminary X-ray diffraction analysis of the TNF–TNFR2 complex are described. The TNF–TNFR2 complex, which comprises one TNF trimer and three TNFR2 monomers, was confirmed and purified by size-exclusion chromatography. Crystals of the TNF–TNFR2 complex were obtained using polyethylene glycol 3350 as a precipitant. The crystal belonged to space group $P2_12_12_1$, with unit-cell parameters a = 74.5, b = 117.4, c = 246.8 Å. Assuming the presence of two TNF–TNFR2 complexes in the asymmetric unit, the Matthews coefficient V_M was 2.49 Å^3 Da^{-1} and the solvent content of the crystal was 50.7%. The crystal diffracted to 2.95 Å resolution.

1. Introduction

Tumour necrosis factor α (TNF) is a major inflammatory cytokine that plays a central role in host defence and inflammation (Aggarwal, 2003). Overexpression of TNF is closely associated with inflammatory diseases such as rheumatoid arthritis and inflammatory bowel disease (Feldmann & Maini, 2003). Therefore, anti-TNF antibodies and soluble TNF receptors (TNFR) that interfere with the activity of TNF have been used to treat various inflammatory diseases (Feldmann, 2002). However, anti-TNF therapy inhibits both types of TNFR (TNFR1 and TNFR2), often causing serious side effects.

Previous studies using animal models of diseases such as arthritis and hepatitis have demonstrated that TNFR1 plays a predominant role in the pathogenesis and exacerbation of inflammation (Mori *et al.*, 1996; Leist *et al.*, 1995). In contrast, TNFR2 is crucial for the proliferation, activation and antigen presentation of T cells, which are essential processes in the cell-mediated immune response against bacteria and viruses (Kafrouni *et al.*, 2003; Grell *et al.*, 1998). Therefore, blocking TNFR1-mediated signal transduction has emerged as a potential therapeutic strategy against inflammatory diseases with a low risk of side effects. Modelling the three-dimensional structure of the TNF–TNFR complex and understanding the differences between TNFR1 and TNFR2 will strongly contribute to the development of a TNFR1-selective therapeutic strategy.

To date, two crystal structures of TNFR1 have been reported: unliganded extracellular domains (PDB codes 1ncf and 1ext; Naismith *et al.*, 1995, 1996) and a lymphotoxin α (LT-α)–TNFR1 complex (PDB code 1tnr; Banner *et al.*, 1993). The structure of wild-type TNF has also been reported (PDB code 1tnf; Eck & Sprang, 1989). Several structures of TNF mutants, including the TNF mutant used in this experiment, have also been reported (PDB codes 1a8m, 2az5, 4tsv, 5tsw, 2e7a and 2zjc; Reed *et al.*, 1997; Cha *et al.*, 1998; Shibata *et al.*, 2008; Mukai *et al.*, 2009). However, the structure of TNFR2 has not yet been reported, although the structure of a viral protein with homology to TNFR2 has been solved (PDB code 2uwi; Graham *et al.*, 2007). This hinders the design of a structure-based drug for advanced anti-TNF therapy. Here, we describe the formation, crystallization and preliminary X-ray diffraction analysis of the

TNF–TNFR2 complex as part of our studies to determine the novel TNFR2 structure and aid in the development of TNFR1-selective therapies.

2. Methods

2.1. Preparation of TNF and TNFR2

The TNF molecule used in this experiment was a Lys-deficient TNF mutant [mutTNF Lys(−); K11M, K65S, K90P, K98R, K112N and K128P] created from wild-type TNF (wtTNF; NCBI accession No. X01394; Uniprot reference P01375) using a phage display system. This mutant retained full bioactivity and affinity for TNFR, as described previously (Yamamoto *et al.*, 2003). The wtTNF–TNFR2 complex formed efficiently, similar to that of mutTNF Lys(−) and TNFR2, but did not crystallize under the conditions described below.

MutTNF Lys(−) (residues 77–233 in Uniprot P01375; 157 amino acids, without tags) was expressed in *Escherichia coli* and refolded from inclusion bodies as described previously (Yamamoto *et al.*, 2003). Briefly, TNF was produced in *E. coli* BL21 (DE3) as inclusion bodies, which were washed in a buffer containing Triton X-100 and solubilized in 6 *M* guanidine–HCl, 0.1 *M* Tris–HCl pH 8.0 and 2 m*M* EDTA. Solubilized protein at 10 mg ml^{-1} was reduced with 65 m*M* dithioerythritol and refolded by a 100-fold dilution in a refolding buffer (100 m*M* Tris–HCl, 2 m*M* EDTA, 0.5 *M* arginine and 0.9 m*M* oxidized glutathione). After dialysis against 20 m*M* Tris–HCl pH 7.4 containing 100 m*M* urea, active trimeric proteins were purified by ion-exchange chromatography using Q-Sepharose FF (GE Healthcare Ltd). Size-exclusion chromatography was performed using a Superose 12 column (GE Healthcare) equilibrated with 20 m*M* Tris–HCl pH 7.4. The molecular mass of the purified TNF trimer was 51 kDa. The complete sequence of this TNF molecule was as follows: VRSSSRTPSD**M**PVAHVVANPQAEGQLQWLNRRANALLANG-VELRDNQLVVPSEGLYLIYSQVLF**S**GQGCPSTHVLLTHTISRI-AVSYQT**P**VNLLSAI**R**SPCQRETPEGAEA**N**PWYEPIYLGGVFQ-LE**P**GDRLSAEINRPDYLDFAESGQVYFGIIAL (residues mutated from wtTNF are shown in bold).

The extracellular domain of TNFR2 was used in this experiment (soluble TNFR2; NCBI accession No. M32315; Uniprot reference P20333). Purified soluble TNFR2 (residues 33–205 in Uniprot P20333; 173 amino acids, without tags) expressed in *E. coli* was purchased from PeproTech Inc. The molecular mass was 19 kDa as a monomer. The complete sequence of this TNFR2 molecule was as follows: APEPGSTCRLREYYDQTAQMCCSKCSPGQHAKVFC-TKTSDTVCDSCEDSTYTQLWNWVPECLSCGSRCSSDQVETQ-ACTREQNRICTCRPGWYCALSKQEGCRLCAPLRKCRPGFG-VARPGTETSDVVCKPCAPGTFSNTTSSTDICRPHQICNVVAIP-GNASMDAVCTSTSP. Lyophilized TNFR2 was dissolved in 20 m*M* Tris–HCl pH 7.4 and used directly for complex formation.

2.2. Purification of the TNF–TNFR2 complex

It is known that one TNF trimer binds three TNFR2 monomers and forms the TNF–TNFR2 complex. For crystallization of the complex, we attempted to purify the full 110 kDa TNF–TNFR2 complex (one 51 kDa TNF trimer and three 19 kDa soluble TNFR2 monomers). The complex was formed by mixing TNF and TNFR2 for 30 min at room temperature. Complex solutions with various molar ratios of TNF and TNFR2 were prepared and the molecular masses were assessed by analytical gel-filtration chromatography using a tandem Superdex 75 10/300 GL/Superdex 200 10/300 GL column (GE Healthcare) in 20 m*M* Tris–HCl pH 7.4 (Fig. 1). The use of two gel-filtration columns with different exclusion limits was useful for separating the complex from uncomplexed TNF and TNFR2. In this analysis, low-molecular-weight and high-molecular-weight gel-filtration calibration kits (GE Healthcare) were used as protein standards. An increase in the mixing ratio of TNFR2 induced a shift

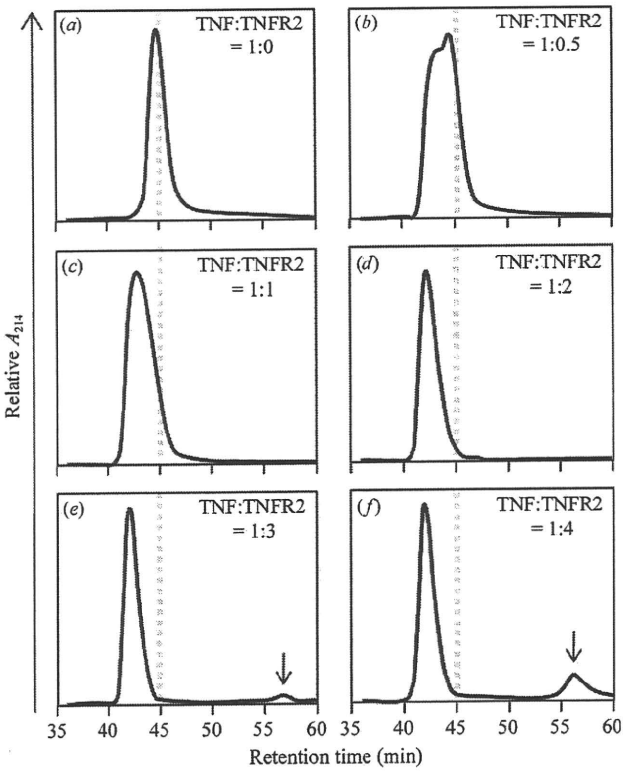

Figure 1
TNF–TNFR2 complex formation. Formation of the TNF–TNFR complex was assessed by analytical gel-filtration chromatography. The molar ratio of TNF trimer and TNFR2 was varied and the elution peak of the proteins was followed at 214 nm. The elution time of uncomplexed TNF occurs at 45 min (*a*). This is indicated by the broken grey line in (*a*)–(*f*). Excess unbound TNFR2 is indicated by arrows in (*e*) and (*f*).

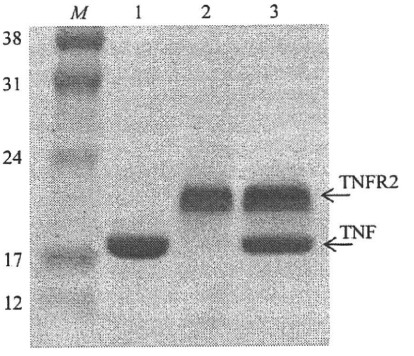

Figure 2
SDS–PAGE analysis of the TNF–TNFR2 complex. Formation of the TNF–TNFR2 complex was confirmed by SDS–PAGE. 15% polyacrylamide gel (ATTO Corp., Tokyo, Japan) was used to separate the bands containing TNF monomer (17 kDa) and TNFR2 monomer (19 kDa). *M*, Rainbow protein standard (labelled in kDa; GE Healthcare); lane 1, 2 µg TNF; lane 2, 2 µg TNFR2; lane 3, 4 µg purified TNF–TNFR2 complex.

in the retention peak of TNF to a higher molecular weight. At a TNF:TNFR2 ratio of 1:3 (Fig. 1*e*), a small peak at 57 min elution time corresponding to unbound 19 kDa TNFR2 was observed. This peak containing excess TNFR2 was also observed at a 1:4 ratio (Fig. 1*f*). This result indicated that the full 110 kDa TNF–TNFR2 complex was formed under these conditions. Therefore, final fractionation was performed between 41 and 44 min at a TNF:TNFR2 ratio of 1:4. The complex formation in the purified fraction was also confirmed by SDS–PAGE (Fig. 2). This full TNF–TNFR2 complex was concentrated to 10 mg ml^{-1} in 20 m*M* Tris–HCl pH 7.4 and used for crystallization as described below. The protein concentration was determined using Coomassie Protein Assay Reagent (Thermo Fisher Scientific Inc.).

2.3. Crystallization of the TNF–TNFR2 complex

The sparse-matrix screening kit Crystal Screen HT and the systematic salt and PEG screening kit Index HT (Hampton Research, Aliso Viejo, California, USA) were used for initial crystallization trials using the sitting-drop vapour-diffusion method. Drops consisting of 0.5 µl protein solution (10 mg ml^{-1}) and 0.5 µl reservoir solution were equilibrated against 100 µl reservoir solution in a Crystal*EX* 96-well flat-bottom plate (Corning Incorporated, Corning, New York, USA). Two temperatures, 293 and 277 K, were tested. Microcrystals were obtained using reservoir solution containing 20%(*w*/*v*) PEG 3350 and 0.2 *M* sodium formate at 293 K. A grid screen around these conditions was evaluated using the hanging-drop vapour-diffusion method. In this step, a drop consisting of 1 µl protein solution and 1 µl reservoir solution was equilibrated against 250 µl reservoir solution in a 24-well VDX Plate (Hampton Research). The crystallization conditions were improved using an additive screening kit (Hampton Research) and round-edged plate-shaped crystals were obtained from a droplet consisting of 1 µl 5 mg ml^{-1} protein solution and 1 µl reservoir solution containing 8%(*w*/*v*) PEG 3350, 0.2 *M* sodium formate and 0.02 *M* cobalt(II) chloride as an additive reagent. Protein and additive concentrations were optimized and the best crystals were obtained using 7.5 µl 0.8 mg ml^{-1} protein solution and 7.5 µl reservoir solution containing 7.5%(*w*/*v*) PEG 3350, 0.2 *M* sodium formate and 0.06 *M* cobalt(II) chloride. The crystals used for data collection had typical dimensions of 0.2 × 0.1 × 0.03 mm (Fig. 3).

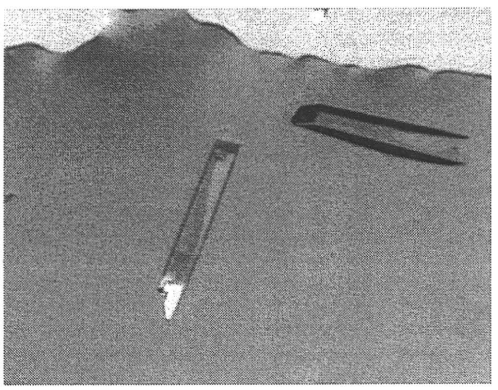

Figure 3
TNF–TNFR2 crystals. Two crystals of the TNF–TNFR2 complex with approximate dimensions of 0.2 × 0.1 × 0.03 mm are shown.

Table 1
Data-collection statistics for the TNF–TNFR2 complex.

Values in parentheses are for the highest resolution shell.

X-ray source	SPring-8 BL41XU
Wavelength (Å)	1.000
Space group	$P2_12_12_1$
Unit-cell parameters	a = 74.5, b = 117.4, c = 246.8
Resolution range (Å)	50–2.95 (3.06–2.95)
Observed reflections	744297
Unique reflections	45945 (4075)
Completeness (%)	98.9 (89.8)
$R_{\rm merge}$† (%)	0.183 (0.603)
$\langle I/\sigma(I)\rangle$	10.75 (1.51)

† $R_{\rm merge} = \sum_{hkl}\sum_i |I_i(hkl) - \langle I(hkl)\rangle| / \sum_{hkl}\sum_i I_i(hkl)$, where $I_i(hkl)$ is the ith intensity measurement of reflection hkl, including symmetry-related reflections, and $\langle I(hkl)\rangle$ is its average.

2.4. Preliminary X-ray analysis

X-ray diffraction experiments were performed on BL41XU of the SPring-8 Synchrotron Facility in Harima, Japan. An ADSC Quantum 315 X-ray CCD detector was installed on BL41XU and used to record the diffraction data. Crystals were soaked in a cryoprotectant solution composed of 7.5%(*w*/*v*) PEG 3350, 0.2 *M* sodium formate, 0.06 *M* cobalt(II) chloride and 30% glycerol. The crystals were then mounted in nylon loops (Hampton Research) and flash-cooled in a nitrogen stream at 95 K. Diffraction data were collected in 1.0° oscillation steps (180 images, 0–180°) and the crystal diffracted X-rays to 2.95 Å resolution. The data set was processed and scaled using the *HKL*-2000 program (Otwinowski & Minor, 1997). The crystals belonged to space group $P2_12_12_1$, with unit-cell parameters a = 74.5, b = 117.4, c = 246.8 Å. Data-collection statistics are shown in Table 1.

3. Results and discussion

The results of SDS–PAGE using the crystallization solution suggested that the crystal contained both TNF and TNFR2. Gel-filtration analysis showed that the TNF–TNFR2 complex with a molecular mass of 110 kDa contained both a TNF trimer (51 kDa) and three TNFR2 monomers (3 × 19 kDa). This suggests that the asymmetric unit of the crystals contained two molecules of the TNF–TNFR2 complex (two TNF trimers and six TNFR2 monomers). The calculated solvent content was 50.7% and the Matthews coefficient was 2.49 Å^3 Da^{-1} (Matthews, 1968).

Molecular replacement was performed with the *MOLREP* program (Vagin & Teplyakov, 1997) in *CCP*4*i* (Potterton *et al.*, 2003) using the TNF mutant structure described in our previous report (PDB code 2e7a; Shibata *et al.*, 2008) as a search model. Two significant solutions corresponding to TNF trimers were obtained (R = 0.469). The model from molecular replacement was subjected to rigid-body refinement, simulated annealing, energy minimization and B-factor refinement using *CNS* (Brünger *et al.*, 1998). The initial electron-density map calculated using only the phases of refined TNF trimer structures (R = 0.425 and $R_{\rm free}$ = 0.493) clearly showed almost the entire TNF trimer. The main chains and side chains of TNFR2 could also be detected around the TNF trimer. Manual model building of TNFR2 based on the TNFR1 structure using the *Coot* program (Emsley & Cowtan, 2004) in *CCP*4*i* is in progress.

This study was supported by Research for Promoting Technological Seeds (No. 11-067) from the Japan Science and Technology Agency (JST), Research Fund Project on Health Sciences focusing on Drug Innovation (No. KAA3701) from the Japan Health Sciences

Foundation, grants from the Ministry of Health, Labor and Welfare in Japan, a Grant-in-Aid for Young Scientists (B) (No. 20790134) and Grants-in-Aid for Scientific Research (Nos. 17016084, 17689008, 17790135, 18015055, 18659047, 20015052 and 20200017) from the Ministry of Education, Culture, Sports, Science and Technology of Japan (MEXT) and Research Fellowships for Young Scientists (No. 20-3919) from Japan Society for the Promotion of Science (JSPS). This study was also supported by Hayashibara Biochemical Laboratories Inc., Okayama, Japan.

References

Aggarwal, B. B. (2003). *Nature Rev. Immunol.* **3**, 745–756.
Banner, D. W., D'Arcy, A., Janes, W., Gentz, R., Schoenfeld, H. J., Broger, C., Loetscher, H. & Lesslauer, W. (1993). *Cell*, **73**, 431–445.
Brünger, A. T., Adams, P. D., Clore, G. M., DeLano, W. L., Gros, P., Grosse-Kunstleve, R. W., Jiang, J.-S., Kuszewski, J., Nilges, M., Pannu, N. S., Read, R. J., Rice, L. M., Simonson, T. & Warren, G. L. (1998). *Acta Cryst.* D**54**, 905–921.
Cha, S. S., Kim, J. S., Cho, H. S., Shin, N. K., Jeong, W., Shin, H. C., Kim, Y. J., Hahn, J. H. & Oh, B.-H. (1998). *J. Biol. Chem.* **273**, 21253–21260.
Eck, M. J. & Sprang, S. R. (1989). *J. Biol. Chem.* **264**, 17595–17605.
Emsley, P. & Cowtan, K. (2004). *Acta Cryst.* D**60**, 2126–2132.
Feldmann, M. (2002). *Nature Rev. Immunol.*, **2**, 364–371.
Feldmann, M. & Maini, R. N. (2003). *Nature Med.* **9**, 1245–1250.
Graham, S. C., Bahar, M. W., Abrescia, N. G., Smith, G. L., Stuart, D. I. & Grimes, J. M. (2007). *J. Mol. Biol.* **372**, 660–671.
Grell, M., Becke, F. M., Wajant, H., Mannel, D. N. & Scheurich, P. (1998). *Eur. J. Immunol.* **28**, 257–263.
Kafrouni, M. I., Brown, G. R. & Thiele, D. L. (2003). *J. Leukoc. Biol.* **74**, 564–571.
Leist, M., Gantner, F., Jilg, S. & Wendel, A. (1995). *J. Immunol.* **154**, 1307–1316.
Matthews, B. W. (1968). *J. Mol. Biol.* **33**, 491–497.
Mori, L., Iselin, S., De Libero, G. & Lesslauer, W. (1996). *J. Immunol.* **157**, 3178–3182.
Mukai, Y., Shibata, H., Nakamura, T., Yoshioka, Y., Abe, Y., Nomura, T., Taniai, M., Ohta, T., Ikemizu, S., Nakagawa, S., Tsunoda, S., Kamada, H., Yamagata, Y. & Tsutsumi, Y. (2009). *J. Mol. Biol.* **30**, 1121–1129.
Naismith, J. H., Devine, T. Q., Brandhuber, B. J. & Sprang, S. R. (1995). *J. Biol. Chem.* **270**, 13303–13307.
Naismith, J. H., Devine, T. Q., Kohno, T. & Sprang, S. R. (1996). *Structure*, **4**, 1251–1262.
Otwinowski, Z. & Minor, W. (1997). *Methods Enzymol.* **276**, 307–326.
Potterton, E., Briggs, P., Turkenburg, M. & Dodson, E. (2003). *Acta Cryst.* D**59**, 1131–1137.
Reed, C., Fu, Z. Q., Wu, J., Xue, Y. N., Harrison, R. W., Chen, M. J. & Weber, I. T. (1997). *Protein Eng.* **10**, 1101–1107.
Shibata, H. *et al.* (2008). *J. Biol. Chem.* **283**, 998–1007.
Vagin, A. & Teplyakov, A. (1997). *J. Appl. Cryst.* **30**, 1022–1025.
Yamamoto, Y., Tsutsumi, Y., Yoshioka, Y., Nishibata, T., Kobayashi, K., Okamoto, T., Mukai, Y., Shimizu, T., Nakagawa, S., Nagata, S. & Mayumi, T. (2003). *Nature Biotechnol.* **21**, 546–552.

J. Biochem. 2009;146(2)167–172
doi:10.1093/jb/mvp065

Fast Binding Kinetics and Conserved 3D Structure Underlie the Antagonistic Activity of Mutant TNF: Useful Information for Designing Artificial Proteo-Antagonists

Yohei Mukai[1,2], Teruya Nakamura[3], Yasuo Yoshioka[2,4], Hiroko Shibata[2], Yasuhiro Abe[2], Tetsuya Nomura[1,2], Madoka Taniai[5], Tsunetaka Ohta[5], Shinsaku Nakagawa[1], Shin-ichi Tsunoda[2], Haruhiko Kamada[2], Yuriko Yamagata[3] and Yasuo Tsutsumi[1,2,*]

[1]Graduate School of Pharmaceutical Sciences, Osaka University, 1-6 Yamadaoka, Suita, Osaka 565-0871; [2]Laboratory of Pharmaceutical Proteomics, National Institute of Biomedical Innovation (NiBio), Osaka 567-0085; [3]Graduate School of Pharmaceutical Sciences, Kumamoto University, Kumamoto 862-0973; [4]The Center for Advanced Medical Engineering and Informatics, Osaka University, 1-6 Yamadaoka, Suita, Osaka 565-0871; and [5]Hayashibara Biochemical Laboratories, Inc., 1-2-3 Shimoishii, Okayama 702-8006, Japan

Received February 18, 2009; accepted March 17, 2009; published online April 22, 2009

Tumour necrosis factor (TNF) is an important cytokine that induces an inflammatory response predominantly through the TNF receptor-1 (TNFR1). A crucial strategy for the treatment of many autoimmune diseases, therefore, is to block the binding of TNF to TNFR1. We previously identified a TNFR1-selective antagonistic mutant TNF (R1antTNF) from a phage library containing six randomized amino acid residues at the receptor-binding site (amino acids 84–89). Two R1antTNFs, R1antTNF-T2 (A84S, V85T, S86T, Y87H, Q88N and T89Q) and R1antTNF-T8 (A84T, V85P, S86A, Y87I, Q88N and T89R), were successfully isolated from this library. Here, we analysed R1antTNF-T8 using surface plasmon resonance spectroscopy and X-ray crystallography to determine the mechanism underlying the antagonistic activity of R1antTNF. The kinetic association/dissociation parameters of R1antTNF-T8 were higher than those of wild-type TNF, indicating more rapid bond dissociation. X-ray crystallographic analysis suggested that the binding mode of the T89R mutation changed from a hydrophobic to an electrostatic interaction, which may be responsible for the antagonistic behaviour of R1antTNF. Knowledge of these structure–function relationships will facilitate the design of novel TNF inhibitors based on the cytokine structure.

Key words: antagonistic activity, mutant, structure–function relationship, tumour necrosis factor (TNF), X-ray crystallography.

Tumour necrosis factor (TNF) is an important immunity-modulating cytokine that is required for human body's defence against infectious diseases and carcinogenesis (*1*). Excess TNF, however, causes various autoimmune diseases, such as rheumatoid arthritis, Crohn's disease and ulcerative colitis. Anti-TNF antibodies and soluble TNF receptors (TNFR), which interfere with the activity of TNF, are currently used to treat various inflammatory diseases (*2–4*). Unfortunately, however, because these therapies also inhibit the TNF-host defence function of the patients, they can cause serious side effects, such as bacterial and viral infection, lymphoma development and lupus inflammatory disease (*5–7*). TNF-blockade in patients with multiple sclerosis can aggravate their symptoms (*8*). TNF exerts its biologic functions by binding to two receptor subtypes, p55 TNFR (TNFR1) and p75 TNFR (TNFR2) (*9*). Many autoimmune diseases related to TNF are triggered by the activation of TNFR1, therefore selective TNFR1 blockade may be a useful therapeutic strategy (*10*). Towards this aim, we previously isolated a TNFR1-selective antagonistic TNF mutant (R1antTNF) using a phage display system (*11*).

In our previous report, we constructed a phage library that displays structural variants of the human TNF in which random amino acids were exchanged for the six residues (amino acids 84–89) predicted to be in the TNF receptor-binding site based on the crystal structure of the lymphotoxin-α (LT-α)–TNFR1 complex (*12*). To isolate a TNFR1-selective mutant TNF antagonist, the phage library, comprising 1×10^7 independent clones, was subjected to two rounds of affinity panning against the human TNFR1 (hTNFR1). Although many of the isolated phage clones induced strong cytotoxicity, some phage clones had almost no cytotoxicity but still had a significant affinity for TNFR1. These non-toxic antagonist candidates (10 clones) were assessed further. The bioactivities and antagonistic activities of recombinant candidates expressed in *Escherichia coli* were measured using the highly TNF-sensitive tumorigenic murine fibroblast cells, L–M cells. Clones T2, T6, T7 and T8 did not activate TNFR1, even when tested at high

*To whom correspondence should be addressed.
Tel: +81-6-6879-8230, Fax: +81-6-6879-8234,
E-mail: ytsutsumi@phs.osaka-u.ac.jp

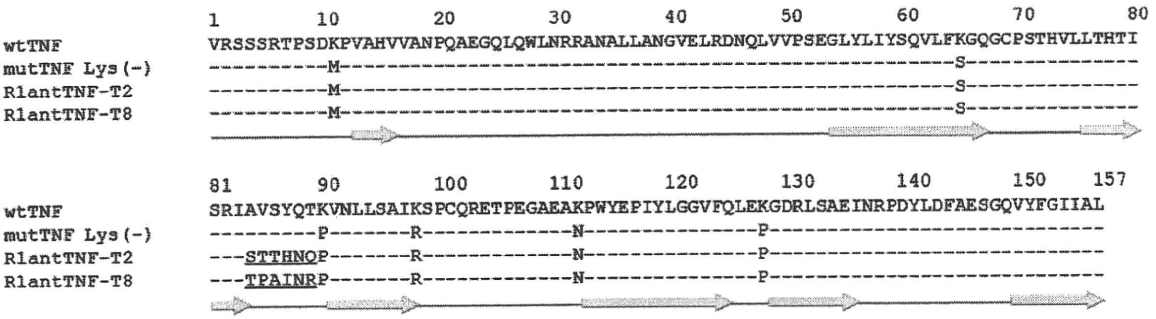

Fig. 1. **Sequence alignment of R1antTNFs and wtTNF.** R1antTNF-T8 and R1antTNF-T2 were created using a phage display system based on a previously reported Lys-deficient TNF mutant (mutTNF Lys(−); K11M, K65S, K90P, K98R, K112N and K128P) (*14*). mutTNF Lys(−) retained full bioactivity and affinity to TNFR. R1antTNFs were mutated in residues 84–89 (underlined), the receptor binding loop. The secondary structure is shown below the TNF sequence (β-sheet; arrow, loop; line).

concentrations, whereas clones T2, T7 and T8 efficiently inhibited wild-type (wt) TNF-induced cytotoxicity. Furthermore, clones T2 and T8 did not bind to TNFR2, suggesting that they were TNFR1-selective antagonists with no bioactivity or affinity for TNFR2. Clones T2 and T8 were renamed R1antTNF-T2 and R1antTNF-T8, respectively, and their sequences are shown in Fig. 1.

As wtTNF converts to an antagonistic TNF by mutation of only six residues, an analysis of the structure–function relationship of R1antTNF will provide important information for the design of artificial TNF inhibitors. Our previous X-ray crystallography and kinetic analysis of the mechanism of antagonism by R1antTNF-T2 suggest that R1antTNF-T2 has higher association/dissociation parameters for TNFR1 binding, despite its similar overall structure to wtTNF (*11*). Based on this finding, we hypothesized that the rapid dissociation of R1antTNF-T2 did not allow for the initiation of an adequate TNFR1 signal.

Here, we show the crystal structure and kinetic properties of another antagonistic TNF, R1antTNF-T8, to support this hypothesis. An understanding of the structure and function of these R1antTNFs, combined with bioinformatics techniques may potentially lead to the design of a functional protein, peptide or peptide mimic that will accelerate the development of novel therapeutic strategies against disease-related proteins, such as TNF.

MATERIALS AND METHODS

Expression and Purification of TNFs—The protocol for the expression and purification of recombinant protein used was the same as that described previously (*13*, *14*). Briefly, TNFs were produced in the *E. coli* BL21 (DE3) strain. The inclusion body of each TNF mutant was washed in Triton X-100 and solubilized in 6 M guanidine–HCl, 0.1 M Tris–HCl, pH 8.0 and 2 mM EDTA. Solubilized protein at 10 mg/ml was reduced with 10 mg/ml dithioerythritol for 4 h at room temperature and refolded by 100-fold dilution in a refolding buffer [100 mM Tris–HCl, 2 mM EDTA, 0.5 M arginine and oxidized glutathione (551 mg/l)]. After dialysis with 20 mM Tris–HCl, pH 7.4, containing 100 mM urea, active trimeric proteins were purified by ion exchange chromatography using Q-Sepharose FF (GE Healthcare Ltd). Size-exclusion chromatography was performed using a Superose 12 column (GE Healthcare Ltd). Endotoxin levels of purified TNF mutants were less than 300 pg/mg.

Kinetic Analysis Using Surface Plasmon Resonance (SPR)—The binding kinetics of TNFs was analysed using the BIAcore 3000 SPR system (GE Healthcare Ltd). Human TNFR1-Fc (hTNFR1) and mouse TNFR1-Fc (mTNFR1; ALEXIS Corporation, Switzerland) were immobilized on a CM5 sensor chip, resulting in an increase of 3000–5000 resonance units. During the association phase, TNF mutants or wtTNF diluted in the running buffer (HBS-EP) at 78.4 nM, 26.1 nM or 8.7 nM were individually passed over the immobilized TNFR at a flow rate of 20 μl/min. During the dissociation phase, the HBS-EP buffer was applied to the sensor chip at a flow rate of 20 μl/min. The data were analysed with BIAEVALUATION 3.0 software (GE Healthcare Ltd) using a 1:1 binding model.

Crystallization—Purified R1antTNF-T8 was concentrated to 10 mg/ml in 20 mM Tris–HCl pH 7.4. Initial screening using a Hampton Crystal Screen 1-2 and Crystal Screen Lite kit (Hampton Research Corporation, Aliso Viejo, CA) was performed using the vapour-diffusion method with hanging drops at 293 K. Drops consisting of 1 μl protein solution (10 mg/ml) and 1 μl reservoir solution were equilibrated against 250 μl reservoir solution in a 24-well VDX™ Plate (Hampton Research Corp.) Micro crystals were obtained with reservoir solution containing 18% PEG_{8000}, 0.2 M calcium acetate hydrate and 0.1 M sodium cacodylate pH 6.5. Reservoir solutions of PEG length and concentration were optimized. The final condition was determined with 1 μl of 10 mg/ml protein solution and 1 μl of reservoir solution containing 15% PEG_{1500}, 0.2 M calcium acetate hydrate and 0.1 M sodium cacodylate pH 6.5. Typical dimensions of the crystals used for data collection were $0.6 \times 0.3 \times 0.3$ (mm^3).

Data Collection and Refinement—X-ray diffraction experiments were performed at BL41XU of the large synchrotron radiation facility, SPring-8, in Harima, Japan. A cryoprotectant solution consisting of 15% PEG_{1500}, 0.2 M calcium acetate hydrate, 20% glycerol and 0.1 M

Table 1. **Crystallographic parameters and refinement statistics of the R1-6 crystal.**

Data collection	
Resolution (Å)	55.7–2.80 (2.90–2.80)
Cell constants (Å)[a]	49.57,111.33,75.38
Space group	$P2_12_12_1$
Measured reflections	36,333
Unique reflections	10,337 (930)
Completeness (%)	92.9 (85.6)
R_{merge} (%)[b]	0.244 (0.530)
I/σ (I)	36.4 (3.16)
Refinement statistics	
Resolutions (Å)	50.0–2.80
Reflections used	9762
R_{cryst} (%)[c]	0.269
R_{free} (%)[d]	0.309
Completeness (%)	90.4
Atoms	
Protein; water	3312; 7
RMSD from ideal	
Bond lengths (Å); bond angles (°)	0.0124; 1.90
B-factor r.m.s. deviation (Å^2)	
Main-chain bonds; side-chain	2.18; 2.58
Main-chain angles; side-chain	4.01; 4.43
Ramachandran plot statistics	
Most favoured regions (%)	75.8
Additionally allowed regions (%)	21.4
Generously allowed regions (%)	2.8
Disallowed regions (%)	0.0

Values in parentheses are those for the outer shell. [a]Cell constants are a, b and c. [b]R_{merge}. $\Sigma|I-<I>|/\Sigma<I>$, where I is intensity of the observations. [c]R_{cryst}. $\Sigma||F_o|-|F_c||/\Sigma|F_o|$, where F_o and F_c are the observed and calculated structure factors, respectively. [d]R_{free} is calculated as for R_{cryst}, but for the test set comprising reflections not used in refinement.

sodium cacodylate pH 6.5 was added to each crystallization drop. The crystals were then mounted in nylon loops (Hampton Research Corp.) and flash-cooled in a nitrogen stream at 95 K. Diffraction data were collected in 1.0° oscillation steps and the crystal diffracted X-rays to a 2.8 Å resolution. The data set was processed and scaled using the program HKL2000 (*15*). The crystals belonged to space group $P2_12_12_1$, with unit-cell parameters $a=49.6$, $b=111.3$ and $c=75.4$Å. Molecular replacement was performed by the Molrep Program in ccp4i (*16*) using a crystal structure of the wtTNF (1TNF) (*17*) as a search model. Cycles of manual rebuilding using the O program (*18*) and refinement using the CNS program (*19*) led to a refined structure. Final model validation was performed using the Procheck Program in ccp4i. Results of the model validation using the Procheck program were as follows: 75.8% residues in the most favoured regions; 21.4% residues in the additional allowed regions; 2.8% residues in the generously allowed regions and 0.0% residues in the disallowed regions. The data collection and refinement statistics are shown in Table 1. The model complexes of TNF–TNFR1 and R1antTNF-T8–TNFR1 were constructed based on the crystal structure of the LT-α–TNFR1 complex (*12*) using the superimposing program in ccp4i.

Table 2. **Kinetic parameters of wtTNF and R1antTNF-T8: affinity to human TNFRI (upper panel) and affinity to mouse TNFRI (lower panel).**

	wtTNF	R1antTNF-T8
Human TNFR1-Fc		
k_{on}[a] ($\times 10^4 M^{-1}S^{-1}$)	4.46	85.30
k_{off}[b] ($\times 10^{-5} S^{-1}$)	8.17	81.90
K_D[c] ($\times 10^{-9}$ M)	1.76	0.96
Mouse TNFR1-Fc		
K_{on}[a] ($\times 10^6 m^{-1}S^{-1}$)	1.30	5.61
k_{off}[b] ($\times 10^{-6} S^{-1}$)	1.06	273.67
K_D[c] ($\times 10^{-11}$ M)	0.08	0.48

[a]Association rate constant. [b]Dissociation rate constant. [c]Equilibrium dissociation constant (k_{off}/k_{on}). Each value was calculated by BIAcore 3000 and BIA evaluation 3.0 software.

RESULTS

Kinetic Analysis of R1antTNF-T8 Using SPR—The kinetic properties of R1antTNF-T8 were compared to those of hTNFR1 and mTNFR1 using the BIAcore 3000 SPR system (Table 2). The dissociation constant (K_D) of R1antTNF-T8 binding to hTNFR1 was similar to that of the wtTNF, although R1antTNF-T8 had no bioactivity through activation of TNFR1, as described previously (*11*). The dissociation kinetic constants (k_{off}) of R1antTNF-T8 for the human and mouse TNFR1 Fc (hTNFR1: $81.9\times10^{-4}s^{-1}$, mTNFR1: $273.7\times10^{-4}s^{-1}$) were clearly higher than those of wtTNF (hTNFR1: $8.17\times10^{-4}s^{-1}$, mTNFR1: $1.06\times10^{-4}s^{-1}$). Interestingly, they were also higher than those of R1antTNF-T2 (hTNFR1: $28.7\times10^{-4}s^{-1}$, mTNFR1: $96.6\times10^{-4}s^{-1}$) previously described (*11*). The association kinetic constants (k_{on}) of R1antTNF for hTNFR1 and mTNFR1 were also higher than those of wtTNF.

R1antTNF-T8 Structure—The overall structures of the R1antTNF-T8 (PDB code: 2ZPX) and wtTNF (PDB code: 1TNF) trimers were similar and superimposed with a root mean square deviation (rmsd) of 1.08 Å for 420 Cα atoms (Fig. 2a). The structure of each monomer of R1antTNF-T8 was similar (rmsd 0.43–0.59 for 140 Cα atoms), as is the case for the wtTNF trimer (*17*). This structural property is similar to that of R1antTNF-T2 (Fig. 2b). In addition, the overall structures of R1antTNF-T8 and R1antTNF-T2 are similar with an rmsd of 0.89 Å for 420 Cα atoms, suggesting that the common structure of the two R1antTNFs may be an important feature for their antagonistic TNF activity.

It is believed that TNF signalling is initiated by the formation of a complex with three TNFR on the cell surface. However, R1antTNFs cannot trigger TNF signal-retaining binding affinity to TNFR1 (Table 2) (*11*). This finding supports the idea that the shared structural/kinetic properties between R1antTNF-T8 and R1antTNF-T2 underlie their TNF antagonistic activity.

DISCUSSION

Kinetic analysis and X-ray crystallography studies of R1antTNF-T8, a TNFR1-selective antagonistic TNF mutant, were performed to determine the mechanism of its antagonistic activity. We previously reported that R1antTNFs have unique properties in that it does not

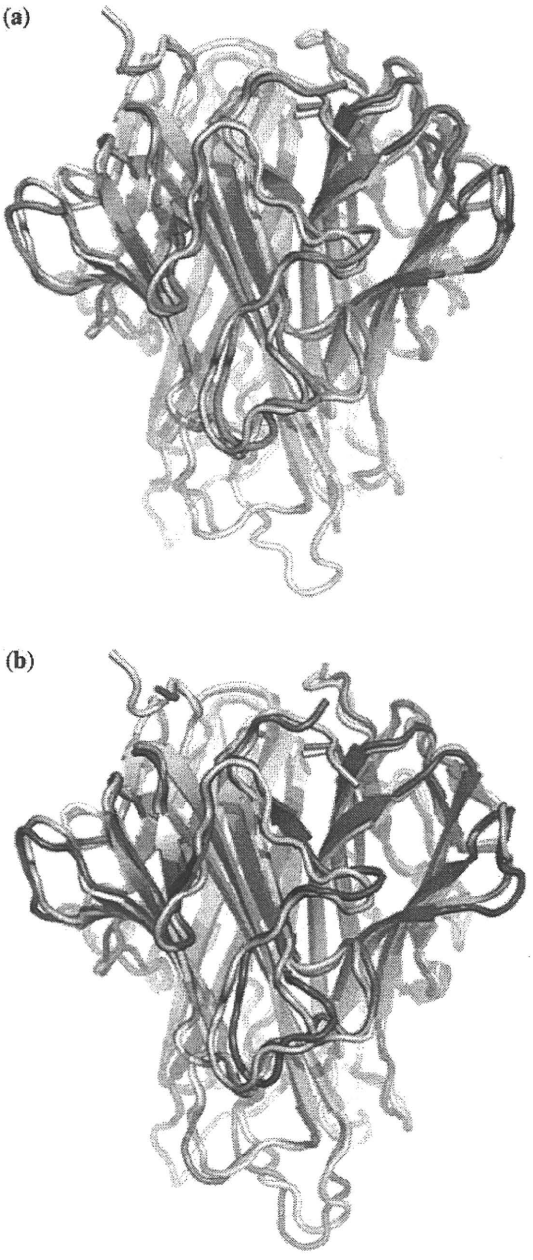

Fig. 2. **Overall structure of wtTNF, R1antTNF-T8 and R1antTNF-T2.** (a) Merged image of previously reported wtTNF structure (grey, 1TNF) and refined R1antTNF-T8 structure (green, 2ZPX). (b) Merged image of wtTNF structure (grey, 1TNF) and R1antTNF-T2 (blue, 2E7A). The flexible loop containing residues 102–110 shown at the bottom of the figure was disordered in the R1antTNF structures. Superimposition of the structures of the wtTNF and R1antTNF was performed using the ccp4i program.

activate TNFR1 despite binding to TNFR1 (*11*). This property allows the mutant TNF to selectively inhibit the TNFR1 signal, which may lead to the design of an effective anti-inflammatory therapy with fewer side effects (*20*). The elucidation of this mechanism will provide useful information for creating novel artificial mutant proteins and inhibitors.

Kinetic analysis of R1antTNF-T8 by SPR indicated that the association and dissociation kinetics are considerably higher than those of wtTNF, indicating that wtTNF and R1antTNF-T8 have different binding patterns. Similar result was also obtained in the case of R1antTNF-T2 (*11*), which suggest that the two R1antTNFs interact with TNFR1 by rapid, repetitive binding and dissociation, and have a binding mode different from that of wtTNF. In addition, the overall structure of R1antTNF-T8 is similar to that of wtTNF and R1antTNF-T2. The structure suggests that R1antTNFs are able to form the TNF–TNFR1 complex for signal initiation without inducing a signal (Fig. 3a) and indicates that R1antTNFs have a different binding mode to TNFR1, an idea supported by their rapid kinetic properties. Because biologically active wtTNF and mutTNF Lys(−) do not show these rapid kinetics, this may be the specific underlying mechanism of the antagonistic activity of R1antTNFs.

To further evaluate the binding pattern, TNF–TNFR1 docking simulation was performed by superimposition. From the model complex of wtTNF–TNFR1, Tyr87 of wtTNF, an essential residue for TNFR1 binding (*21*), was buried in a molecular hydrophobic 'pocket' of TNFR1 in which the receptor residues Leu67 and Leu71 are located (Fig. 3b). Tyr87 in R1antTNF-T8 and R1antTNF-T2 was used to replace other amino acids (Ile87 and His87, respectively; Fig. 3c and d). The structural simulation revealed that Arg89 of R1antTNF-T8 and His87 of R1antTNF-T2 interacted with the relatively negatively charged Ser63 and Asn65 on the TNFR1 surface, which may account for the difference in the association mode compared to wtTNF (Fig. 3c and d). The change from a hydrophobic interaction (Y87) to an electrostatic interaction (Y87H and Y87I/T89R) could cause the unstable, rapid TNFR1 binding pattern that is common to both R1antTNFs.

Furthermore, it is also interesting that the position of a key mutational residue is different in each R1antTNF (Arg89 of R1antTNF-T8 and His87 of R1antTNF-T2). It is thought that we successfully isolated these different R1antTNFs because we used the combinatorial phage library of six randomized amino acids (residues 84–89). From this result, we can also reconfirm that phage display is a powerful tool for isolating mutant proteins that are difficult to design using traditional point mutation methods (*11*, *14*, *22*).

The fact that the rapid binding pattern of these TNF mutants influenced their signal transduction function will be useful for designing artificial drugs and developing more precise tools for basic research. This report also suggested that the fusion of bioinformatics and kinetic/structural analyses would enhance the development of various therapeutic molecules.

FUNDING

Research for Promoting Technological Seeds (No. 11-067) from the Japan Science and Technology Agency (J.S.T.);

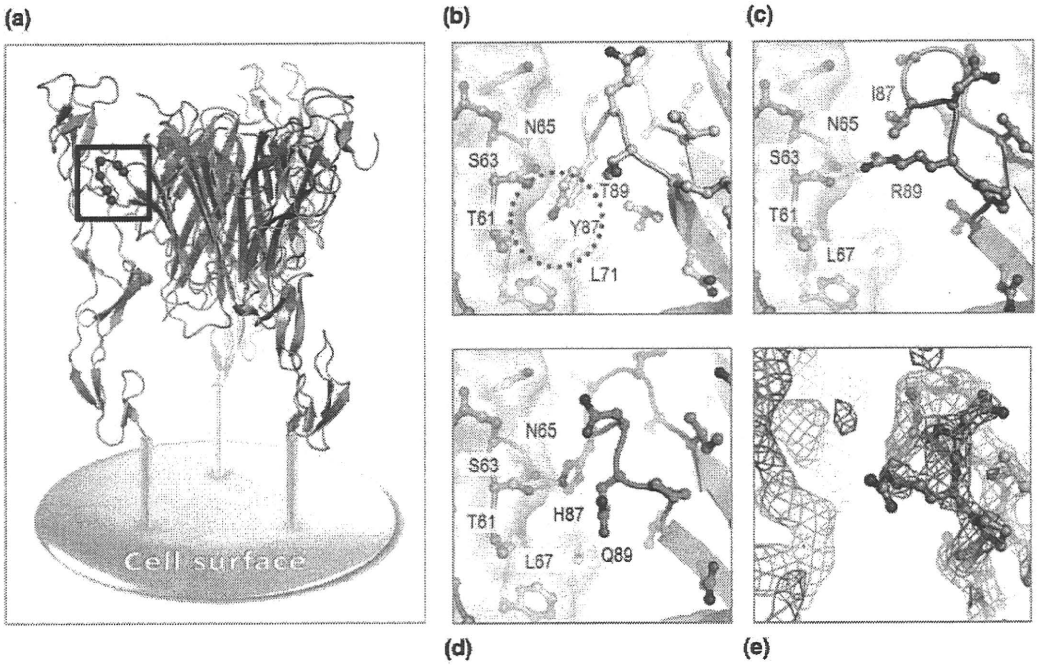

Fig. 3. **Predicted binding model of R1antTNF and TNFR1.** (a) Model complex of R1antTNF-T8 (2ZPX; green cartoon) and TNFR1 (red cartoon) on the cell surface. This complex was built with the Superpose application of the ccp4i program using the LT-α–TNFR1 complex (1TNR). Receptor-binding interfaces corresponding to Fig. 3b–e are indicated by the black square. Mutated residues (amino acids at positions 84–89) are shown as red spheres. (b–d) Receptor-binding interfaces of (b) wtTNF–TNFR1 (grey–red), (c) R1antTNF-T8–TNFR1 (green–red) and (d) R1antTNF-T2–TNFR1 (blue–red). These models were also built with the Superpose application (wtTNF; 1TNF, R1antTNF-T8; 2ZPX, R1antTNF-T2; 2E7A). Critical hydrophobic interaction of wtTNF Y87 and TNFR1 is indicated by the orange circle. In this simulation, the side chains of each structure were rotated to fit the predicted interaction. Stable structures of these rotamers were constructed using the O program. Potential interactions are indicated by yellow dashed lines. (e) 2Fo-Fc map contoured at 0.9 σ of R1antTNF-T8 loop (pink mesh).

Research Fund Project on Health Sciences focusing on Drug Innovation (No. KAA3701) from the Japan Health Sciences Foundation; Grants from the Ministry of Health, Labor and Welfare in Japan; Grant-in-Aid for Young Scientists (B) (No. 20790134) and Grants-in-Aid for Scientific Research (Nos. 17016084, 17689008, 17790135, 18015055, 18659047, 20015052 and 20200017) from the Ministry of Education, Culture, Sports, Science and Technology of Japan (MEXT); Research Fellowships for Young Scientists (No. 20-3919) from Japan Society for the Promotion of Science (JSPS).

CONFLICT OF INTEREST

None declared.

REFERENCES

1. Aggarwal, B.B. (2003) Signalling pathways of the TNF superfamily: a double-edged sword. *Nat. Rev. Immunol.* **3**, 745–756
2. Feldmann, M. and Maini, R.N. (2003) Lasker Clinical Medical Research Award. TNF defined as a therapeutic target for rheumatoid arthritis and other autoimmune diseases. *Nat. Med.* **9**, 1245–1250
3. Rutgeerts, P., Van Assche, G., and Vermeire, S. (2004) Optimizing anti-TNF treatment in inflammatory bowel disease. *Gastroenterology* **126**, 1593–1610
4. Kooloos, W.M., de Jong, D.J., Huizinga, T.W., and Guchelaar, H.J. (2007) Potential role of pharmacogenetics in anti-TNF treatment of rheumatoid arthritis and Crohn's disease. *Drug Discov. Today* **12**, 125–131
5. Keane, J., Gershon, S., Wise, R.P., Mirabile-Levens, E., Kasznica, J., Schwieterman, W.D., Siegel, J.N., and Braun, M.M. (2001) Tuberculosis associated with infliximab, a tumor necrosis factor alpha-neutralizing agent. *N. Engl. J. Med.* **345**, 1098–1104
6. Shakoor, N., Michalska, M., Harris, C.A., and Block, J.A. (2002) Drug-induced systemic lupus erythematosus associated with etanercept therapy. *Lancet* **359**, 579–580
7. Nathan, D.M., Angus, P.W., and Gibson, P.R. (2006) Hepatitis B and C virus infections and anti-tumor necrosis factor-alpha therapy: guidelines for clinical approach. *J. Gastroenterol. Hepatol.* **21**, 1366–1371
8. Sicotte, N.L. and Voskuhl, R.R. (2001) Onset of multiple sclerosis associated with anti-TNF therapy. *Neurology* **57**, 1885–1888
9. Aggarwal, B.B., Eessalu, T.E., and Hass, P.E. (1985) Characterization of receptors for human tumour necrosis factor and their regulation by gamma-interferon. *Nature* **318**, 665–667
10. Kollias, G. and Kontoyiannis, D. (2002) Role of TNF/TNFR in autoimmunity: specific TNF receptor blockade may be advantageous to anti-TNF treatments. *Cytokine Growth Factor Rev.* **13**, 315–321

11. Shibata, H., Yoshioka, Y., Ohkawa, A., Minowa, K., Mukai, Y., Abe, Y., Taniai, M., Nomura, T., Kayamuro, H., Nabeshi, H., Sugita, T., Imai, S., Nagano, K., Yoshikawa, T., Fujita, T., Nakagawa, S., Yamamoto, A., Ohta, T., Hayakawa, T., Mayumi, T., Vandenabeele, P., Aggarwal, B.B., Nakamura, T., Yamagata, Y., Tsunoda, S., Kamada, H., and Tsutsumi, Y. (2008) Creation and X-ray structure analysis of the tumor necrosis factor receptor-1-selective mutant of a tumor necrosis factor-alpha antagonist. *J. Biol. Chem.* **283**, 998–1007
12. Banner, D.W., D'Arcy, A., Janes, W., Gentz, R., Schoenfeld, H.J., Broger, C., Loetscher, H., and Lesslauer, W. (1993) Crystal structure of the soluble human 55 kd TNF receptor-human TNF beta complex: implications for TNF receptor activation. *Cell* **73**, 431–445
13. Mukai, Y., Shibata, H., Nakamura, T., Yoshioka, Y., Abe, Y., Nomura, T., Taniai, M., Ohta, T., Ikemizu, S., Nakagawa, S., Tsunoda, S., Kamada, H., Yamagata, Y., and Tsutsumi, Y. (2009) Structure–function relationship of tumor necrosis factor (TNF) and its receptor interaction based on 3D structural analysis of a fully active TNFR1-selective TNF mutant. *J. Mol. Biol.* **385**, 1221–1229
14. Yamamoto, Y., Tsutsumi, Y., Yoshioka, Y., Nishibata, T., Kobayashi, K., Okamoto, T., Mukai, Y., Shimizu, T., Nakagawa, S., Nagata, S., and Mayumi, T. (2003) Site-specific PEGylation of a lysine-deficient TNF-alpha with full bioactivity. *Nat. Biotechnol.* **21**, 546–552
15. Otwinowski, Z. and Minor, W. (1997) Processing of X-ray diffraction data collected in oscillation mode. *Methods Enzymol.* **276**, 307–326
16. Potterton, E., Briggs, P., Turkenburg, M., and Dodson, E. (2003) A graphical user interface to the CCP4 program suite. *Acta Crystallogr. D Biol. Crystallogr.* **59**, 1131–1137
17. Eck, M.J. and Sprang, S.R. (1989) The structure of tumor necrosis factor-alpha at 2.6 A resolution. Implications for receptor binding. *J. Biol. Chem.* **264**, 17595–17605
18. Jones, T.A., Zou, J.Y., Cowan, S.W., and Kjeldgaard, M. (1991) Improved methods for building protein models in electron density maps and the location of errors in these models. *Acta Crystallogr. A* **47**, 110–119
19. Brunger, A.T., Adams, P.D., Clore, G.M., DeLano, W.L., Gros, P., Grosse-Kunstleve, R.W., Jiang, J.S., Kuszewski, J., Nilges, M., Pannu, N.S., Read, R.J., Rice, L.M., Simonson, T., and Warren, G.L. (1998) Crystallography & NMR system: a new software suite for macromolecular structure determination. *Acta Crystallogr. D Biol. Crystallogr.* **54**, 905–921
20. Shibata, H., Yoshioka, Y., Ohkawa, A., Abe, Y., Nomura, T., Mukai, Y., Nakagawa, S., Taniai, M., Ohta, T., Mayumi, T., Kamada, H., Tsunoda, S., and Tsutsumi, Y. (2008) The therapeutic effect of TNFR1-selective antagonistic mutant TNF-α in murine hepatitis models. *Cytokine* **44**, 229–233
21. Zhang, X.M., Weber, I., and Chen, M.J. (1992) Site-directed mutational analysis of human tumor necrosis factor-alpha receptor binding site and structure–functional relationship. *J. Biol. Chem.* **267**, 24069–24075
22. Shibata, H., Yoshioka, Y., Ikemizu, S., Kobayashi, K., Yamamoto, Y., Mukai, Y., Okamoto, T., Taniai, M., Kawamura, M., Abe, Y., Nakagawa, S., Hayakawa, T., Nagata, S., Yamagata, Y., Mayumi, T., Kamada, H., and Tsutsumi, Y. (2004) Functionalization of tumor necrosis factor-alpha using phage display technique and PEGylation improves its antitumor therapeutic window. *Clin. Cancer Res.* **10**, 8293–8300

Biochemical and Biophysical Research Communications 388 (2009) 667–671

Contents lists available at ScienceDirect

Biochemical and Biophysical Research Communications

journal homepage: www.elsevier.com/locate/ybbrc

Novel protein engineering strategy for creating highly receptor-selective mutant TNFs

Tetsuya Nomura [a,b,1], Yasuhiro Abe [a,1], Haruhiko Kamada [a,c], Masaki Inoue [a], Tomoyuki Kawara [a,b], Shuhei Arita [a,b], Takeshi Furuya [a,b], Yasuo Yoshioka [b,c], Hiroko Shibata [a], Hiroyuki Kayamuro [a,b], Takuya Yamashita [a,b], Kazuya Nagano [a], Tomoaki Yoshikawa [a,b], Yohei Mukai [b], Shinsaku Nakagawa [b,c], Madoka Taniai [d], Tsunetaka Ohta [d], Shin-ichi Tsunoda [a,b,c,*], Yasuo Tsutsumi [a,b,c]

[a] National Institute of Biomedical Innovation (NiBio), 7-6-8 Saito-Asagi, Ibaraki, Osaka 567-0085, Japan
[b] Graduate School of Pharmaceutical Sciences, Osaka University, 1-6 Yamadaoka, Suita, Osaka 565-0871, Japan
[c] The Center for Advanced Medical Engineering and Informatics, Osaka University, 1-6 Yamadaoka, Suita, Osaka 565-0871, Japan
[d] Hayashibara Biochemical Laboratories Inc., 675-1 Fujisaki, Okayama 702-8006, Japan

ARTICLE INFO

Article history:
Received 4 August 2009
Available online 13 August 2009

Keywords:
Tumor necrosis factor (TNF)
Gene shuffling
Phage display technique
Protein engineering
TNF receptor-selective mutant

ABSTRACT

Tumor necrosis factor (TNF) plays important roles in host defense and in preventing tumor formation by acting via its receptors, TNFR1 and TNFR2, functions of which are less understood. To this end, we have been isolating TNF receptor-selective mutants using phage display technique. However, generation of a phage library with large repertoire (>10^8) is impeded by the limited transformation efficiency of *Escherichia coli*. Therefore, it is currently difficult to create a mutant library containing amino acid substitutions in more than seven residues. To overcome this problem, here we have used two different TNF mutant libraries, each containing random substitutions at six selected amino acid residues, and utilized a gene shuffling method to construct a randomized mutant library containing substitutions at 12 different amino acid residues of TNF. Consequently, using this library, we identified TNF mutants with greater receptor-selectivity and enhanced receptor-specific bioactivity than the existing mutants.

Introduction

Tumor necrosis factor-α (TNF) plays a critical role in host defense through regulation of cell survival, death, and inflammation by acting via one of its receptors, TNFR1 and TNFR2 [1]. Because excess or uncontrolled activity of TNF is often a cause for many immunological diseases and tumor development [2,3], biological drugs such as recombinant TNFs (for enhancement of TNF signaling) or anti-TNF monoclonal antibodies (Mab) and soluble TNF receptors (for neutralization of TNF signaling) have made significant impacts in the treatment of inflammatory diseases and in tumor therapy [4,5]. A number of published reports, however, suggested that neutralization of TNF resulted in increased risk of bacterial infection and several other side effects because of the blocking of signaling via both TNFR1 and TNFR2 [4,5]. Therefore, there is an urgent need to fully understand the biology of the TNF receptor mediated signaling pathway and to develop novel drugs for therapeutic use in TNF-related immunological diseases. For this purpose, TNF receptor-knockout mice were used to understand the relationship between the function of the TNF receptors and TNF-related diseases [8–10]. Recently, it was revealed that the two receptors worked together by crosstalk signaling, which suggested that the TNF-mediated signaling in the presence of both TNF receptors actually correlates with their physiological functions [1,6,7]. To elucidate the roles of TNFR1 and TNFR2, many researchers used an agonistic or an antagonistic TNF mutant that selectively binds to one of the receptors and initiates the biological activity of that specific receptor. These mutant TNFs might be a promising new class of TNF-related drugs without any side effect, and could as well serve as a tool for analyzing the receptor function. Development of these mutant TNFs has facilitated understanding of the molecular interaction between the TNF and its receptors, TNFR1 and TNFR2. In this context, it is noteworthy that several approaches have been undertaken to establish quantitative correlation between the receptor subtype specific-biological activity and the structural and kinetic binding parameters of a receptor-specific TNF mutant [8]. Mutational analysis of single amino acid residues revealed that amino acids at positions 15, 31–35, 84–87, 117, 119 and 143–148, which are clustered throughout in hotspots, greatly contributed to the biological activity of TNF [9,10].

* Corresponding author. Address: Laboratory of Pharmaceutical Proteomics, National Institute of Biomedical Innovation, 7-6-8 Saito-Asagi, Ibaraki, Osaka 567-0085, Japan. Fax: +81 72 641 9817.
E-mail address: tsunoda@nibio.go.jp (S.-i. Tsunoda).
[1] These authors contributed equally to the work.

0006-291X/$ - see front matter © 2009 Elsevier Inc. All rights reserved.
doi:10.1016/j.bbrc.2009.08.052